Article:

Barr, A. orcid.org/0000-0002-8240-6412, Rigby, S.E. and Clayton, M. (2020) Correction of higher mode Pochhammer-Chree dispersion in experimental blast loading measurements. International Journal of Impact Engineering, 139. 103526. ISSN 0734-743X

https://doi.org/10.1016/j.ijimpeng.2020.103526

Correction of higher mode Pochhammer–Chree dispersion in experimental blast loading measurements

A. D. Barr[a], S. E. Rigby[a], M. Clayton[a]

[a]*Department of Civil & Structural Engineering, The University of Sheffield, Mappin Street, Sheffield, S1 3JD, UK*

Abstract

Experimental measurements of blast loading using Hopkinson pressure bars are affected by dispersion which can result in the loss or distortion of important high-frequency features. Blast waves typically excite multiple modes of propagation in the bar, and full correction of dispersive effects is not currently possible as the magnitude of stress propagating in each mode is not known. In this paper we develop an algorithm for multiple mode dispersion correction based on rigorous interrogation of the results from a series of finite element analyses. First, a finite element model is validated against first-mode and higher-mode theory. The dispersion of short raised-cosine windowed pulses is then used to isolate the contribution of each propagating mode, enabling a relationship between frequency and modal apportioning of stress to be obtained for the first four propagating modes. Finally, four-mode dispersion correction is successfully applied to an experimental signal using an algorithm based on the derived relationships for modal apportioning. The four-mode results show significant improvement in the capture of high-frequency features over existing first-mode corrections, and demonstrate the potential of this method for the full correction of dispersion in experimental measurements of blast loading.

Keywords: Dispersion correction, Hopkinson pressure bar, Multiple mode, Pochhammer-Chree, LS-DYNA

1. Introduction

The provision of adequate blast protection systems is dependent on our ability to accurately quantify the loading arising from detonation of a high explosive. Blast events present a considerable challenge to the experimentalist: measurement devices should be robust enough to withstand pressures in the range of 10s–100s MPa, whilst being sufficiently sensitive and fast-acting to resolve temporal features in the kHz–MHz range.

The Hopkinson pressure bar [1], or HPB, is commonly used as a dynamic force transducer in investigations of the loading from explosive events, as it combines the durability and sensitivity required to record the high-pressure

Email address: a.barr@sheffield.ac.uk (A. D. Barr)

transient features inherent in blast and shock waves [2–11]. In a HPB, a stress wave applied to one end of the bar propagates down its length, and is recorded by strain gauges fixed to the bar surface some distance away. The wave equations derived by Pochhammer [12] and Chree [13] indicate that each frequency component of a stress wave will propagate at a velocity dependent on the frequency of that component. Thus, a signal will disperse as it propagates from the loaded face of the pressure bar to the strain gauge.

Dispersion of a stress wave is of particular concern in the measurement of explosive events, as it can result in the distortion or loss of important high-frequency features, impeding accurate quantification of the loading [14]. Dispersion of the stress wave is also accompanied by a frequency-dependent variation in stress across the bar cross-section, and so a signal recorded on the bar surface may not be representative of the mean stress in the bar [15–17].

The Pochhammer–Chree equations have an infinite number of roots corresponding to different modes of propagation, so that a high-frequency component may propagate in more than one mode, each with its own phase and group velocities (Figure 1). The transmission of energy in the bar occurs at the group velocity, c_g, while individual wave features, such as a particular crest, propagate at the phase velocity, c_p. While the phase velocity in the higher modes often exceeds c_0 (Figure 1a), the energy associated with these waves will always propagate in the bar at velocities below c_0 (Figure 1b).

When only the first mode of propagation is excited, the frequency domain dispersion correction method developed by Gorham [18] and Follansbee and Frantz [19] can be used. In this method, the fast Fourier transform (FFT) of a signal is taken, the phase angle of each frequency component is adjusted according to the phase velocity derived from the Pochhammer–Chree equations, and an inverse FFT returns the signal to the time domain. Tyas and Watson [20] extended this method to account for the variation of stress across the bar cross-section by applying additional corrections to the amplitude of each frequency component, an approach which was later verified experimentally by Tyas and Pope [21].

Above the cutoff frequency for the second mode of propagation, at least two modes will propagate at any given frequency, and each mode will propagate with a distinct velocity and amplitude. In signals which contain significant high frequency content, such as blast and shock waves, the magnitude of each frequency component therefore represents the sum of the stresses propagating in each mode at that frequency. If the portion of the total stress assigned to each mode is known, the amplitude of each frequency component can be divided amongst

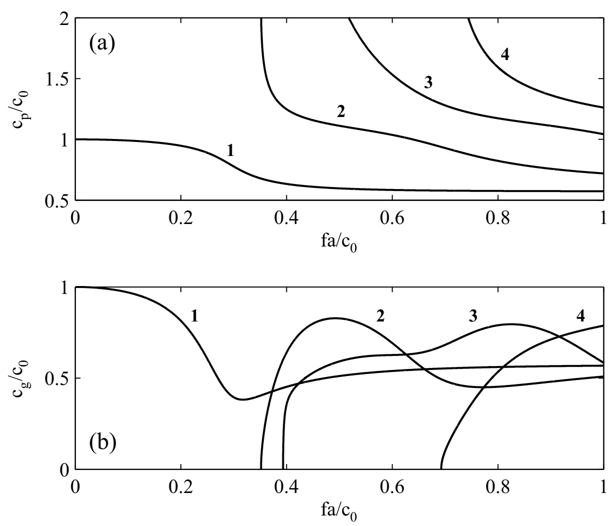

Figure 1: Variation of a) phase velocity, c_p, and b) group velocity, c_g, with frequency for the first four modes of wave propagation in a cylindrical bar (ν = 0.3).

the propagating modes, and then each mode individually corrected for dispersion according to its phase velocity. However, this modal apportioning relationship is not provided by the Pochhammer–Chree curves, and so has been a topic of research for many years.

Gregory and Gladwell [22] analysed the Pochhammer–Chree equations with an integral formulation of least squares to determine the proportion of a sinusoidal wave propagating in each mode at normalised frequencies up to $fa/c_0 \approx 0.40$, where f is frequency, a is the radius of the bar and c_0 is the one-dimensional wave speed. Puckett [23] used this approach to develop an analytical model for wave propagation in cylindrical bars, although comparisons with experimental signals showed that the analytical model could not accurately predict dispersion for wavelengths exceeding the bar diameter, i.e. when higher dispersion modes were excited.

Lee et al. [24, 25] used experimental pressure data with a Gaussian-windowed Fourier transform to estimate the time of arrival and relative power of each frequency component in a blast wave. The results suggested that at a given frequency the mode with the highest group velocity carried the majority of the signal energy. This led to the development of dispersion curves based on the simplification that the entire magnitude of each frequency component only propagates in the mode with the highest group velocity. However, Husemeyer [26] performed multiple-mode dispersion simulations which showed that the contribution of the remaining propagating modes is not sufficiently small to enable them to be neglected in this manner.

Despite a number of previous studies investigating multi-mode dispersion correction, there is no consensus and no proven method to estimate the magnitude of a given frequency component propagating in a given mode, other than for frequencies where only one mode propagates. No researchers to date have successfully isolated each mode of propagation, and the contribution of each mode to a reconstructed (dispersion corrected) pressure signal has yet to be demonstrated. The safe, economical design of blast-resistant structures, the investigation of explosive phenomena at small scaled distances, and the rigorous validation of numerical modelling approaches all depend on the development of reliable methods for the correction of higher-mode dispersive effects in experimental measurements of blast loading.

This paper presents a new method for correcting for dispersion in the first four modes of propagation. First, a finite element model is validated against theoretical predictions of the cross-sectional distribution of stress for single and multiple-mode propagation in a cylindrical bar. The finite element model is then used to derive 'modal apportioning factors' by propagating a windowed single-frequency signal down a HPB and recording amplitudes some distance down the bar, after the signal has separated into distinct modes. Finally, we present modifications to the Tyas and Watson [20] phase angle correction method to account for higher modes, and we present an example of higher-mode dispersion correction of an experimental signal. The contribution of each of the first four modes is calculated up to $fa/c_0 = 0.90$, enabling the correction of multiple-mode dispersion in experimental recordings of the loading from explosive events.

2. Finite element model validation

2.1. Initial considerations

The Pochhammer–Chree equations arise from the application of traction-free boundary conditions to the wave equation,

$$\frac{\partial^2 u}{\partial t^2} = c^2 \nabla^2 u. \tag{1}$$

In a finite element (FE) model of a cylindrical pressure bar, wave propagation is described by this same equation, and so complex phenomena such as multiple-mode propagation, dispersion and cross-sectional variations in stress should arise as predicted by the analytical methods. Finite element methods can therefore be particularly useful for investigating phenomena where the governing relationships are intractable, as in the case of modal stress apportioning.

Results can be obtained over the whole volume and time of interest, as the discretisation allows, however there are known limitations of the FE method which should be considered. The Pochhammer–Chree equations were derived for the case of an infinitely-long pressure bar subjected to an infinitely-long sinusoidal axial disturbance. While it is only possible to model an *approximation* of an infinitely-long pressure bar, the errors introduced by deviating from a *true* infinite bar can be minimised by windowing the forcing functions to reduce the inertial effects[1] introduced by the sudden application of stress at a free face [20, 26], or by enforcing zero displacement boundary conditions for a small length of bar equal to the wavelength of the forcing function [28].

Representation of mass in either a lumped or consistent matrix will give rise to spurious oscillations [29], and the central-differencing explicit time-stepping algorithm used in most finite element solvers will give rise to oscillations that are indistinguishable from Pochhammer–Chree dispersion [28]. The results from a finite element model may therefore begin to diverge from theory, particularly when considering cumulative numerical losses associated with propagating higher frequencies (relative to mesh size) over long distances. However, these errors can be minimized by using smaller, uniformly-sized elements and a time-step that is close to the critical time-step, given as the smallest element length divided by the one-dimensional wave speed.

To ensure that the modal apportioning of stress is accurately calculated by finite element methods, this section first compares the dispersion and radial distribution of stress modelled in LS-DYNA with the theoretical relationships, for both single and multiple mode propagation. The distribution of stress between the propagating modes is a result of the same wave equation responsible for these effects, and so accuracy in these behaviours is a good indicator that modal apportioning is also well captured.

2.2. Propagation in the first mode

Simulations were first compared to the Pochhammer–Chree relationships for situations where the forcing frequency was below the Mode 2 cutoff frequency ($fa/c_0 \approx 0.35$), where it is known that only the first mode will propagate. A cylindrical steel pressure bar was modelled in LS-DYNA [30] with volume-weighted axi-symmetric shell elements and the **MAT_ELASTIC* material model, using the parameters in Table 1 which were informed by previous mesh sensitivity studies [31, 32]. The dispersion of continuous sinusoidal waves of unit amplitude was

[1] When a pulse is applied suddenly to the end of a HPB the majority of the energy propagates axially along the bar. However, a small fraction of the energy remains at the loaded end of the bar in a very narrow frequency band. The energy of this resonant mode gradually leaks into the HPB as a normal propagating mode, known as an ‘evanescent mode’ [27].

	First mode	Higher modes
Element length, mm	0.2	0.4
Bar radius, mm	5	10
Bar length, m	3	10

(a)

Parameter	Value
Young's modulus, GPa	210
Density, Mg/m^3	7.850
Poisson's ratio	0.3

(b)

Table 1: a) Mesh geometry and b) LS-DYNA *Elastic* material model parameters used for analysis of first and higher mode propagation.

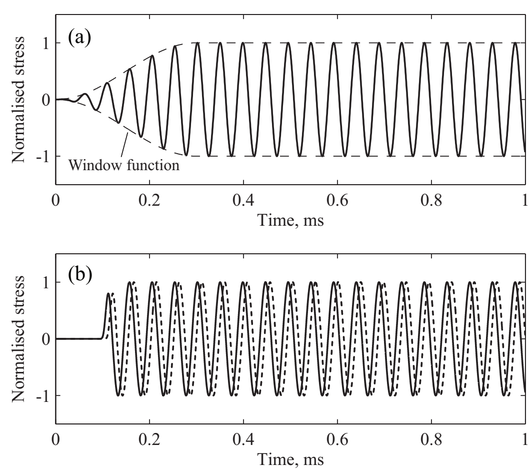

Figure 2: a) Sinusoidal forcing function with half raised-cosine window and b) stress measured on the bar axis 500 mm and 550 mm from the free end, for $fa/c_0 = 0.02$.

then assessed by modelling forcing functions at normalised frequencies up to 0.34 and comparing the resultant phase velocities and cross-sectional variations of stress with those predicted by Pochhammer–Chree theory.

In each case, a sinusoid of unit amplitude was applied to the end of the bar for the entire 1 ms duration of the analysis, representing an infinite duration pulse, with the addition of a 0.3 ms raised-cosine window applied at the beginning of the wave to reduce the inertial effects as discussed above. To ensure that any further inertial effects associated with the head of the applied pulse did not influence the results, results from the early stages of the analysis were omitted. Only the latter stages of the output signals were considered, defined as the region over which the stress response has constant peak amplitude.

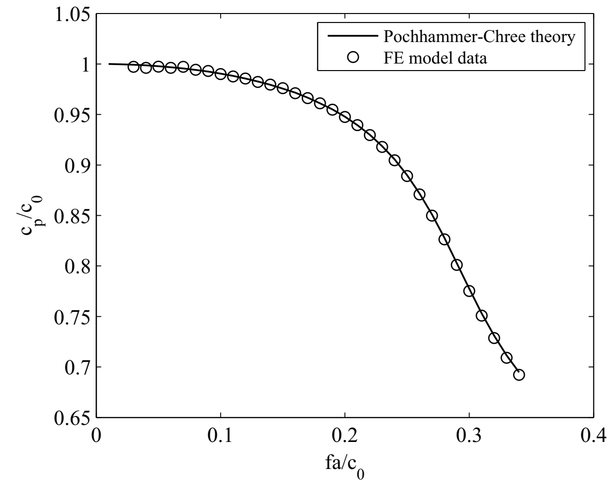

Figure 3: Relationship of phase velocity and frequency for Mode 1: comparison of Pochhammer–Chree theory and FE-modelled pressure bar.

Examples of the forcing function and the stress measured on the bar axis 500 mm and 550 mm from the end are shown in Figure 2. Stresses were calculated by converting the axial component of nodal velocity (v) into axial stress (σ) using the expression $\Delta\sigma = \rho c_0 \Delta v$. Phase velocity was calculated from these measurements by assessing the change in phase angle that occurred between the two measurement locations. Phase velocities for normalised frequencies up to 0.34 are shown in Figure 3, where it can be seen that the numerical results closely match the relationship derived by Davies [15] through manipulation of the Pochhammer–Chree equations.

The distribution of stress across the bar cross-section was investigated in a similar manner for a number of normalised frequencies between 0.09 and 0.34 by recording the stress at various radial ordinates between the bar axis and surface at a location 500 mm from the end of the bar. The measured stresses were normalised against the stress at the bar axis. The results are shown in Figure 4, where again it can be seen that the model is in very good agreement with the Davies [15] theoretical values at each normalised frequency.

2.3. Propagation in higher modes

In order to investigate wave propagation in higher modes, the radius and length of the pressure bar were increased (Table 1). This allowed lower velocity frequency components to reach the monitoring location without any reflected waves arriving from the distal end of the bar and corrupting the results. Thus, the assumption of an infinite-length bar was maintained. A full raised-cosine window was applied to a sinusoid of the required frequency to produce a pulse of 0.2 ms length, as shown in Figure 5a. The wave envelope created by the windowing function

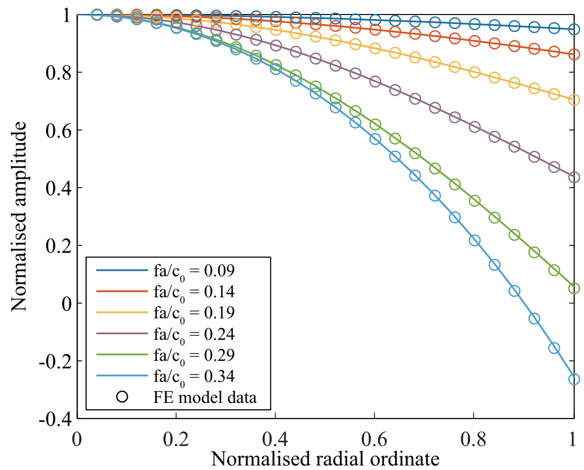

Figure 4: Spatial distribution of stress over the bar cross-section for Mode 1: comparison of Davies' analysis [15] and FE-modelled pressure bar.

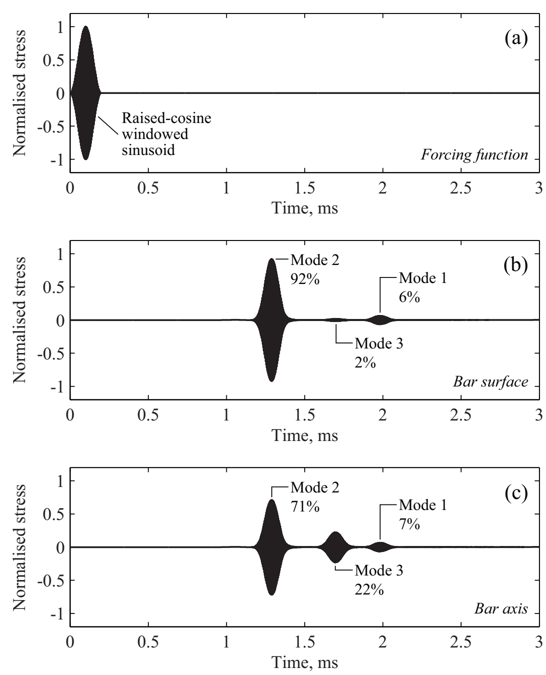

Figure 5: a) Raised-cosine windowed sinusoidal forcing function, and stresses measured after 6.0 m propagation on the bar b) surface and c) axis, for $fa/c_0 = 0.52$.

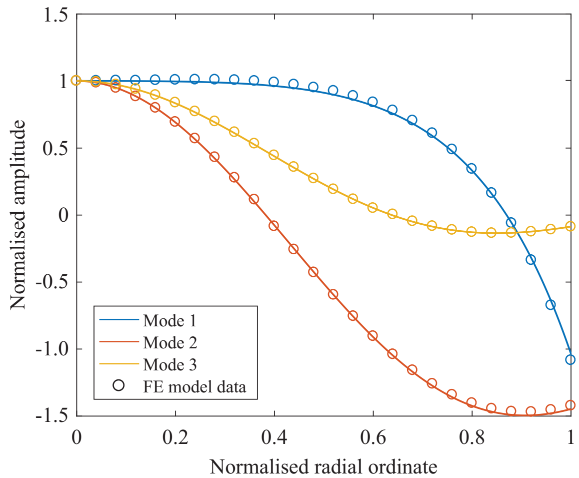

Figure 6: Spatial distribution of stress over the bar cross-section for Modes 1–3 at $fa/c_0 = 0.52$: comparison of Davies' analysis [15] and FE-modelled pressure bar.

propagates in the bar at the group velocity, and so, as each mode propagates at its own group velocity, a single-frequency input pulse will disperse and eventually separate into several distinct pulses, equal to the number of modes present. This effect is shown in Figures 5b and 5c for a sinusoid with a normalised frequency of 0.52, where the signal propagates in Modes 1–3. As a finite-duration input signal was used, at a point 6 m down the bar three separate modes can be clearly distinguished and identified using measurements of group velocity. From this, the relative amplitude of the pulses can be calculated.

The stress propagating in each mode at a particular radial ordinate was taken as the peak value of each distinct modal pulse, and by recording at a variety of radial ordinates, the distribution of stress over the bar cross-section was calculated for each mode. The cross-sectional distributions arising from the forcing function in Figure 5a are shown in Figure 6; these results remain close to the theoretical values obtained from Davies' analysis [15] even though multiple modes are now propagating. This suggests that while numerical errors may be present (Section 2.1), they are insufficient to cause significant deviation from analytical theory. Hence, as LS-DYNA can replicate these dispersive and radial stress distribution effects in waves propagating in higher modes, we can be confident that the proportion of stress associated with each individual mode is also being modelled correctly.

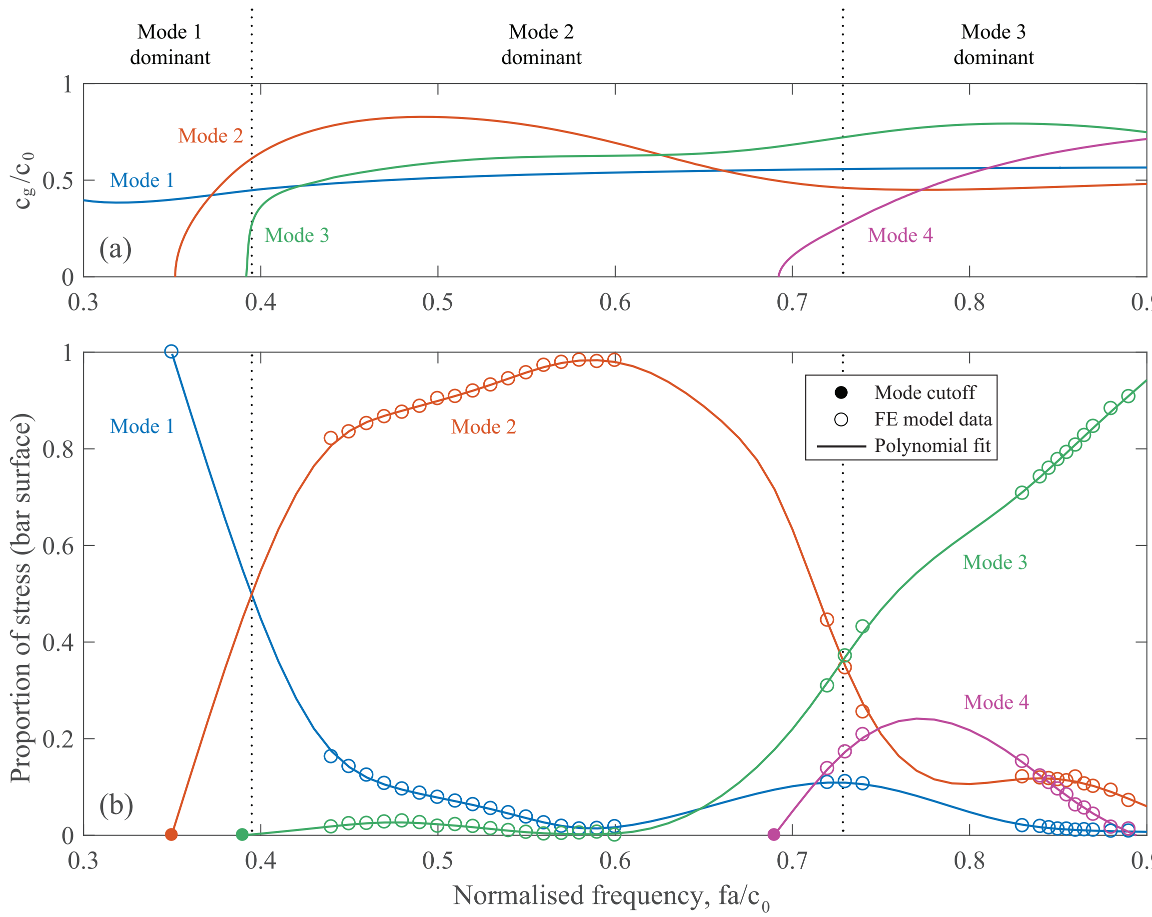

Figure 7: a) Group velocities of Modes 1–4 and b) the proportion of stress travelling in each mode on the bar surface, for $0.30 < fa/c_0 < 0.90$.

3. Derivation of modal apportioning factors

3.1. Modal apportioning factors and graphical representation

Using the method in Section 2.3, the modal distribution of stress measured on the surface of the bar was assessed at a range of normalised frequencies up to 0.90, at which point four modes are propagating simultaneously. The results are shown in Figure 7, where the abscissa denotes the modelled frequency for each separate numerical analysis, and the ordinates represent the contribution of each mode at that frequency. As an example, at $fa/c_0 = 0.52$ the proportion of stress propagating in Modes 1, 2 and 3 is 6%, 92% and 2% respectively, as was previously shown in Figure 5.

At frequencies where the group velocity of two or more modes is similar, the relative dispersion is not large enough for the clear separation of the forcing function into modal pulses. As it is not possible to identify the contribution of individual modes in these cases, the modal stress distribution cannot be resolved at these frequencies using the current method. However, an indication of the behaviour in these regions can be provided using the piecewise polynomial fits shown in Figure 7. Two additional constraints are applied to the fits: the stress propagating in a particular mode is zero below the cutoff frequency of that mode; and the proportions of the propagating modes should sum to unity at any normalised frequency. Any error initially present in the sum of the modes was minimised through iterative distribution between the contributing modes and refitting of the curves, so that even outside the modelled results the error in the sum of the fits remains below 1%. The modal proportions in Figure 7 are provided in a supplementary file [33] as the ratios r_1, r_2, r_3 and r_4, along with the cross-sectional mean for each mode, $\bar{r_1}$, $\bar{r_2}$, $\bar{r_3}$ and $\bar{r_4}$, to enable future investigation and development of further correction algorithms. Results are provided at normalised frequency increments of 0.01, and indicate where the modal contributions are derived directly from the modelling study ('M'), or interpolated from the piecewise polynomial fits ('I').

3.2. Interpretation

The modal apportioning of stress on the bar surface in Figure 7 indicates a gradual transfer of stress from Mode 1 to Mode 2 at frequencies above the Mode 2 cutoff. From approximately $fa/c_0 = 0.40$ the majority of the stress propagates in Mode 2, and this remains the case until $fa/c_0 = 0.73$, where Mode 3 becomes dominant. Mode 4 does not become dominant over the considered frequency range. These results appear to be in good qualitative agreement with the energy partitions of Lamb waves derived in the case of plane strain response of semi-infinite elastic strips to harmonic excitation [34].

Comparison of Figures 7a and 7b indicates that the frequencies over which a particular mode is dominant do not closely relate to the frequencies at which that mode has the highest group velocity, as was reported by Lee et al. [25]. For example, the group velocity of Mode 3 exceeds all other propagating modes from $fa/c_0 = 0.63$, but the proportion of stress propagating in Mode 3 does not exceed that of the other modes until $fa/c_0 = 0.73$. Between these frequencies Mode 2 is also briefly the *slowest* propagating mode while remaining dominant in terms of stress proportion. These results additionally confirm that the magnitudes of the non-dominant modes are not small enough to justify neglecting their contributions, except within narrow frequency bands, as discussed by Husemeyer [26].

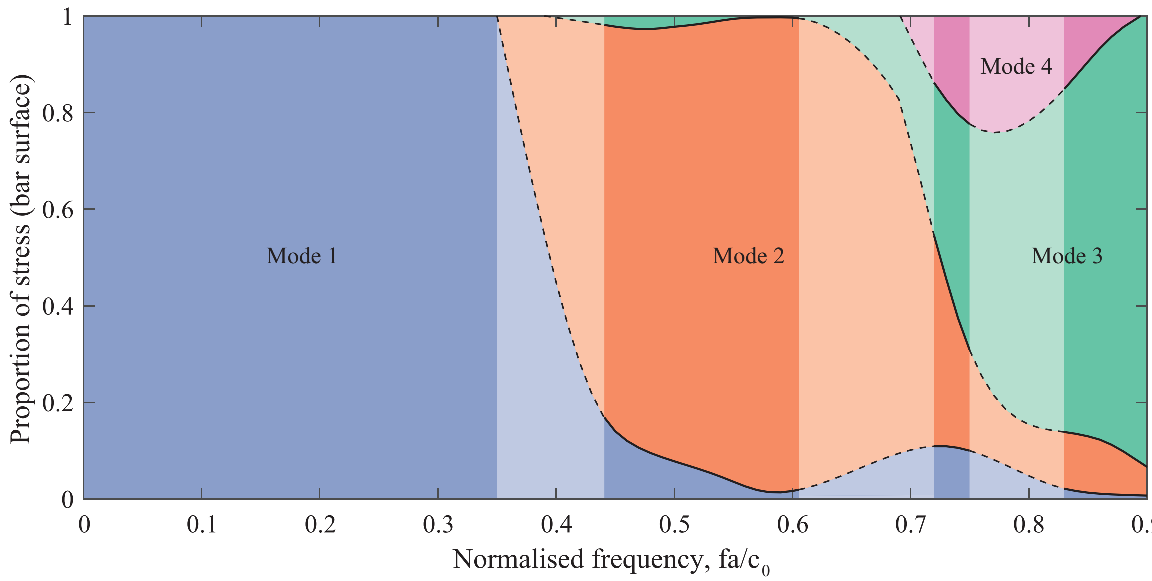

Figure 8: Distribution of stresses across Modes 1–4 for $0 < fa/c_0 < 0.90$. Dashed lines indicate interpolated data.

The data in Figure 7 can also be represented using stacked areas as in Figure 8, which shows how the total stress associated with each propagating frequency component is distributed between the first four modes for normalised frequencies between 0 and 0.90. In this figure the greyed-out areas represent regions where the group velocities of the propagating modes are similar and the modal apportioning relationships have been interpolated from the piecewise polynomial fits, as discussed previously. Successful measurements at these frequencies would require a much longer pressure bar to enable sufficient relative dispersion. This has not been attempted in the current work as the additional length would have introduced significant alteration of the signal through numerical losses.

The modal distribution of stresses in Figure 8 can be used with phase angle adjustments to calculate the stress acting at another point on the bar surface, as in the following example. The next challenge in higher mode dispersion correction will be to consider the radial variation of stress and strain in the bar, using factors M_1 and M_2 for each propagating mode [20]. The values of M_1 and M_2 can be easily derived for any mode, but contain discontinuities at frequencies where nodal cylinders coincide with the bar surface, and so further investigation will be required to quantify the data lost due to these nodal cylinders and develop best practice on their use.

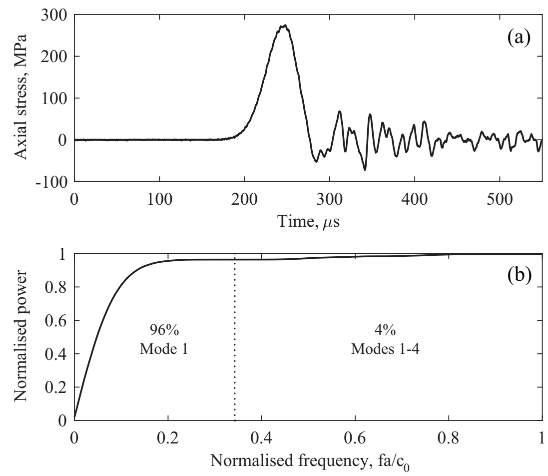

Figure 9: a) A dispersed experimental Hopkinson pressure bar signal and b) the normalised cumulative power with frequency.

4. Higher mode correction of an experimental signal

The numerical results above indicate that it is now possible to determine how a signal will separate into its component modes as it propagates in a Hopkinson pressure bar: this can be demonstrated by applying higher mode correction to an experimental signal. Figure 9a shows a signal recorded 1 m from the end of an explosively-loaded Hopkinson pressure bar used to perform acceleration tests on electronic components at the University of Sheffield Blast & Impact Laboratory in Buxton, UK. The steel pressure bar is 2 m long, 100 mm diameter and has $c_0 = 5185$ m/s and $\nu = 0.3$. The dispersion of the signal is clear from the tail of high-frequency oscillations following the main loading: these oscillations would continue beyond the 550 μs shown here, but are overwritten by the stress wave reflecting from the end of the bar. The cumulative power plot in Figure 9b, determined from an FFT of the recorded signal, indicates that 96% of the signal is at frequencies below the Mode 2 cutoff, and so will propagate in Mode 1 only. The remaining 4% is above the Mode 2 cutoff, and will propagate in two, three or four modes simultaneously.

Correction of this signal was performed to obtain the stress on the surface of the bar at the loaded face, removing the dispersion associated with 1 m of travel. A first-mode dispersion correction program [35, 36] was modified to incorporate the proportion of stress propagating in each of the first four modes, using the values for the bar surface derived in Section 3. The original program uses the method described by Tyas and Watson [20] to apply a phase angle correction to each frequency component, $x(\omega)$,

$$x(\omega) = A(\omega)\, \mathrm{e}^{\mathrm{i}\phi(\omega)} \tag{2}$$

where $A(\omega)$ is the amplitude of the component and $\phi(\omega)$ is the phase angle, and both are functions of the component's angular frequency ω. The phase angle correction, $\phi'(\omega)$, is calculated as

$$\phi'(\omega) = \left(\frac{c_0}{c_p(\omega)} - 1\right) \frac{\omega z}{c_0} \tag{3}$$

where z is the propagation distance to correct over. A modified frequency component, $x'(\omega)$, can then be reconstructed as

$$x'(\omega) = A(\omega)\, \mathrm{e}^{\mathrm{i}(\phi(\omega) - \phi'(\omega))}. \tag{4}$$

To incorporate Modes 2, 3 and 4, phase angle corrections ($\phi'_1(\omega)$, $\phi'_2(\omega)$ etc.) are calculated for each mode according to the phase velocity at that frequency. The modified frequency component is then given as the sum of the portions propagating in each mode, which are scaled by the mode ratios ($r_1(\omega)$, $r_2(\omega)$ etc.) derived in Section 3:

$$x'(\omega) = \sum_{m=1}^{4} r_m(\omega)\, A(\omega)\, \mathrm{e}^{\mathrm{i}(\phi(\omega) - \phi'_m(\omega))}. \tag{5}$$

Figure 10 shows a comparison of one-mode and four-mode dispersion correction of the signal in Figure 9a, where corrections have been applied to remove the dispersion associated with 1 m of travel in the bar. 'One-mode' correction assumes that the total signal at each frequency propagates only at the Mode 1 phase velocity: this is the current limitation imposed on dispersion correction without the modal apportioning factors derived in this paper. While only 4% of the power of the signal is propagating in multiple modes, there is a significant difference in the loading predicted by the two methods.

One-mode correction of the signal reduces the tail of high-frequency components following the main stress wave, but, as all frequencies are assumed to propagate at Mode 1 phase velocities, large oscillations are introduced ahead of and during the signal. For the current signal, one-mode correction remains adequate for non-local measurements, such as total impulse, as the large local errors largely cancel each other out over over the range of interest. For example, the uncorrected signal in Figure 10b has a total impulse of 95.2 N s, while the one-mode and

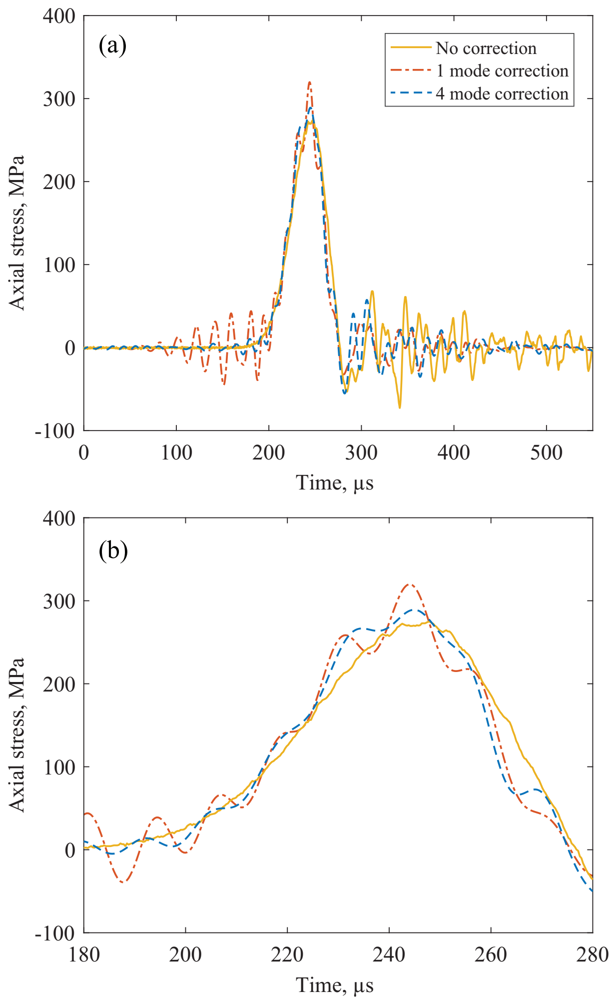

Figure 10: Single-mode and multiple-mode dispersion correction of a Hopkinson pressure bar signal, showing a) the complete signal and b) the main loading wave in detail. The 'no correction' signal is represented by the original recorded signal timeshifted using the one-dimensional wave speed of the bar, c_0.

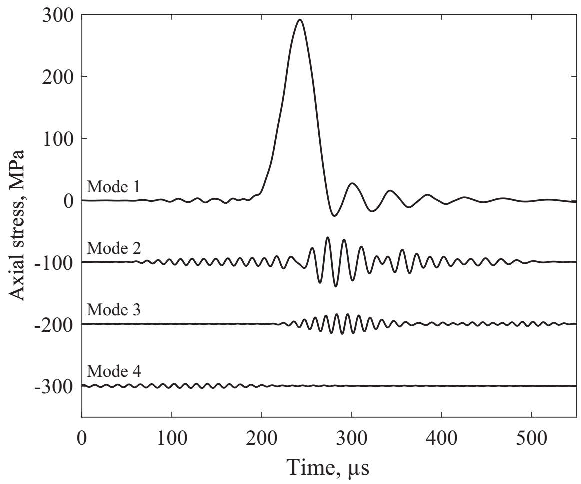

Figure 11: Stress waves propagating in Modes 1–4 in the four-mode corrected signal shown in Figure 10. Modes 2–4 are each offset by -100 MPa for clarity.

four-mode corrected signals have total impulses of 91.9 N s and 92.0 N s, respectively: both methods correct the 4% under-prediction from the recorded signal.

For applications requiring local accuracy of the signal, the correction is greatly improved by the inclusion of the higher modes, which minimise spurious oscillations while resolving the shape and rise time of the main stress wave. For example, the peak overpressure measured by the strain gauge is 275 MPa, and four-mode dispersion correction calculates that this peak would be 289 MPa at the loaded face of the bar. The additional oscillations in the one-mode signal result in a calculated peak overpressure of 320 MPa, over-predicting the four-mode value by 11%.

The contribution of each mode to the four-mode corrected signal is shown in Figure 11. Although the majority of the signal propagates in Mode 1, the waves propagating in higher modes have amplitudes of up to 40 MPa, illustrating why one-mode correction is inadequate in this example. The accurate temporal positioning of the stress in higher modes is of particular importance when identifying key high-frequency features in blast loading recordings, such as rise time, peak overpressure and wave reflections observed within the signal. Without higher-mode correction, these features can appear at the wrong position in the signal, have the wrong magnitude, or be lost altogether due to interference of the frequency components. In the example shown the oscillations following the main wave are not entirely removed by either correction method, but this is likely to be due to the data lost on the arrival of the reflected wave after 550 μs, and experiments could be designed to eliminate this issue.

5. Summary and conclusions

A pressure signal will disperse as it travels down a Hopkinson pressure bar because each component propagates at a velocity which is dependent on its frequency. Whilst methods exist for correcting this dispersion at lower frequencies, above a certain frequency a signal will propagate in multiple modes, at which point existing methods lose accuracy and validity. In this paper, we developed a method for correcting dispersion in higher modes based on a comprehensive numerical study using a validated finite element model.

First, we determined that finite element modelling of a Hopkinson pressure bar could provide quantitative data on the modal distribution of stress with frequency for use in higher-mode dispersion correction. Numerical simulations demonstrated that the dispersion and cross-sectional variation of both single-mode and multiple-mode stress waves in a cylindrical bar were accurately predicted, and so there was confidence that the distribution of stress between modes would also be modelled accurately.

Propagation in higher modes was assessed using short raised-cosine windowed pulses, which dispersed into multiple modal pulses as the signal propagated along the bar, enabling the contribution of each mode to be measured up to a normalised frequency of 0.90. All four modes in this range were shown to contribute significantly at frequencies above their cutoff frequency, and dominance of a mode did not closely relate to group velocity.

Finally, we presented four-mode dispersion correction of an experimental signal. The results showed a marked improvement over the existing single-mode method, highlighting the importance of multi-mode dispersion correction, as well as demonstrating the applicability and validity of finite element modelling as a tool for understanding multi-mode wave propagation behaviour. The dispersion correction algorithm allows for correction of the first four modes, up to normalised frequencies of $fa/c_0 = 0.90$, extending the accuracy and applicability of established frequency-domain techniques well beyond the Mode 2 cutoff frequency of $fa/c_0 \approx 0.35$.

Acknowledgements

This work forms part of a project that was joint-funded by the Defence Science and Technology Laboratory (Dstl) and the Institution of Civil Engineers Research and Development Enabling Fund. The authors wish to thank Matthew Gant and Ian Elgy from Dstl, Professor Harm Askes from the University of Sheffield, and Professor Andrei Metrikine from Delft University of Technology for their helpful comments during preparation of the manuscript.

[1] B. Hopkinson, A method of measuring the pressure produced in the detonation of high explosives or by the impact of bullets, Philosophical Transactions of the Royal Society of London. Series A 213 (1914) 437–456.

[2] L. C. Taylor, W. L. Fourney, H. U. Leiste, Pressures on targets from buried explosions, International Journal for Blasting & Fragmentation 4 (2010) 165–192.

[3] S. Rigby, A. Tyas, S. Clarke, S. Fay, J. Reay, J. Warren, M. Gant, I. Elgy, Observations from Preliminary Experiments on Spatial and Temporal Pressure Measurements from Near-Field Free Air Explosions, International Journal of Protective Structures 6 (2015) 175–190.

[4] S. Clarke, S. Fay, J. Warren, A. Tyas, S. Rigby, I. Elgy, A large scale experimental approach to the measurement of spatially and temporally localised loading from the detonation of shallow-buried explosives, Measurement Science and Technology 26 (2015) 015001.

[5] S. Rigby, S. Fay, S. Clarke, A. Tyas, J. Reay, J. Warren, M. Gant, I. Elgy, Measuring spatial pressure distribution from explosives buried in dry Leighton Buzzard sand, International Journal of Impact Engineering 96 (2016) 89–104.

[6] T. J. Cloete, G. N. Nurick, Blast characterization using a ballistic pendulum with a centrally mounted Hopkinson bar, International Journal of Protective Structures 7 (2016) 367–388.

[7] A. Tyas, J. J. Reay, S. D. Fay, S. D. Clarke, S. E. Rigby, J. A. Warren, D. J. Pope, Experimental studies of the effect of rapid afterburn on shock development of near-field explosions, International Journal of Protective Structures 7 (2016) 456–465.

[8] X. Cui, X. Yao, Y. Chen, A lab-scale experiment approach to the measurement of wall pressure from near-field under water explosions by a Hopkinson bar, Shock and Vibration 8273469 (2018) 1–15.

[9] S. Rigby, S. Fay, A. Tyas, S. Clarke, J. Reay, J. Warren, M. Gant, I. Elgy, Influence of particle size distribution on the blast pressure profile from explosives buried in saturated soils, Shock Waves 28 (2018) 613–626.

[10] X. Yao, K. Cui, X. Guo, Y. Chen, An experimental approach to the measurement of wall pressure generated by an underwater spark-generated bubble by a Hopkinson bar, Shock and Vibration 5341317 (2019) 1–14.

[11] S. E. Rigby, A. Tyas, R. J. Curry, G. S. Langdon, Experimental measurement of specific impulse distribution and transient deformation of plates subjected to near-field explosive blasts, Experimental Mechanics 59 (2019) 163–178.

[12] L. Pochhammer, Über die fortpflanzungsgeschwindigkeiten kleiner schwingungen in einem unbegrenzten isotropen kreiszylinder [About the propagation velocity of small vibrations in an infinite isotropic circular cylinder], Journal für die reine und angewandte Mathematik 81 (1876) 324–336.

[13] C. Chree, The equations of an isotropic elastic solid in polar and cylindrical co-ordinates, Transactions of the Cambridge Philosophical Society 14 (1889) 250–369.

[14] S. Rigby, A. Barr, M. Clayton, A review of Pochhammer-Chree dispersion in the Hopkinson bar, Proceedings of the Institution of Civil Engineers: Engineering and Computational Mechanics 171 (2018) 3–13.

[15] R. M. Davies, A critical study of the Hopkinson Pressure Bar, Philosophical Transactions of the Royal Society of London. Series A. 240 (1948) 375–457.

[16] N. A. Safford, Materials testing up to 10^5 s^{-1} using a miniaturised Hopkinson Bar with dispersion corrections, in: Proceedings of the International Symposium on Intense Dynamic Loading and its Effects, Chengdu, China, 1992.

[17] A. Tyas, A. J. Watson, Experimental evidence of Pochammer-Chree strain variations in elastic cylinders, Experimental Mechanics 40 (2000) 331–337.

[18] D. A. Gorham, A numerical method for the correction of dispersion in pressure bar signals, Journal of Physics E: Scientific Instruments 16 (1983) 477–479.

[19] P. S. Follansbee, C. Frantz, Wave propagation in the Split Hopkinson Pressure Bar, Journal of Engineering Materials and Technology 105 (1983) 61–66.

[20] A. Tyas, A. J. Watson, An investigation of frequency domain dispersion correction of pressure bar signals, International Journal of Impact Engineering 25 (2001) 87–101.

[21] A. Tyas, D. J. Pope, Full correction of first-mode Pochammer-Chree dispersion effects in experimental pressure bar signals, Measurement Science and Technology 16 (2005) 642–652.

[22] R. D. Gregory, I. Gladwell, Axisymmetric waves in a semi-infinite elastic rod, The Quarterly Journal of Mechanics and Applied Mathematics 42 (1989) 327–337.

[23] A. Puckett, An experimental and theoretical investigation of axially symmetric wave propagation in thick cylindrical waveguides, Ph.D. thesis, The Graduate School, The Unversity of Maine, USA, 2004.

[24] C. K. B. Lee, R. C. Crawford, A new method for analysing dispersed bar gauge data, Measurement Science and Technology 4 (1993) 931–937.

[25] C. K. B. Lee, R. C. Crawford, K. A. Mann, P. Coleman, C. Petersen, Evidence of higher Pochhammer-Chree modes in an unsplit Hopkinson Bar, Measurement Science and Technology 6 (1995) 853–859.

[26] P. J. A. Husemeyer, Theoretical and numerical investigation of multiple-mode dispersion in Hopkinson bars, Ph.D. thesis, Blast Impact and Survivability Research Unit, Department of Mechanical Engineering, University of Cape Town, South Africa, 2011.

[27] J. Oliver, Elastic wave dispersion in a cylindrical rod by a wide-band short-duration pulse technique, The Journal of the Acoustical Society of America 29 (1957) 189–194.

[28] R. A. Govender, T. J. Cloete, G. N. Nurick, A numerical investigation of dispersion in Hopkinson pressure bar experiments, Journal de Physique IV 134 (2006) 521–526.

[29] G. Goudreau, R. Taylor, Evaluation of numerical integration methods in elastodynamics, Computer methods in applied mathematics and engineering 2 (1972) 69–97.

[30] J. O. Hallquist, LS-DYNA Theory Manual, Livermore Software Technology Corporation, CA, USA, 2006.

[31] G. Valsamos, F. Casadei, G. Solomos, A numerical study of wave dispersion curves in cylindrical rods with circular cross-section, Applied and Computational Mechanics 7 (2013) 99–114.

[32] A. Tyas, Z. Ozdemir, On backward dispersion correction of Hopkinson pressure bar signals, Philosophical Transactions of the Royal Society of London. Series A, Mathematical, Physical and Engineering Sciences 372 (2014) 20130291.

[33] A. D. Barr, S. E. Rigby, M. Clayton, Data for the proportion of longitudinal stress travelling in Modes 1-4 in a Hopkinson pressure bar, for 0.35 < fa/c0 < 0.90, at the bar surface and as a cross-sectional mean, 2020. doi:10.15131/shef.data.11709978.v1.

[34] B. Karp, Generation of symmetric lamb waves by non-uniform excitations, Journal of Sound and Vibration 312 (2008) 195–209.

[35] A. D. Barr, Dispersion.m – a MATLAB script for phase angle and amplitude correction of pressure bar signals, 2016. doi:10.15131/shef.data.3996876.v1.

[36] A. D. Barr, Strain-rate effects in quartz sand, Ph.D. thesis, Department of Civil & Structural Engineering, University of Sheffield, UK, 2016.